SanDiego SPIE Meeting August 3, 2002 Draft 8June03

Sea Surface Temperature Measurements with AIRS

Hartmut . H. Aumann, Moustafa Chahine and Diana Barron
Jet Propulsion Laboratory, California Institute of Technology, Pasadena CA 91109

Abstract

The comparison of global sea surface skin temperatures derived from cloud-free AIRS super window channel at 2616cm-1 (sst2616) with the Real-Time Global Sea Surface Temperature (RTG.SST) for September 2002 shows a surprisingly small standard deviation of 0.44K, but sst2616 is colder than the RTG.SST by 0.67K. About 0.3K of the cold bias is due the expected bulk-skin gradient and the effect of using the day/night average RTG.SST for a night time comparison. The other 0.37K is due to an absorbing layer in the atmosphere. There are large areas of the oceans where this absorbing layer is absent and others where it is as large at 1.5K. The layers persist regionally on a months time scale and may be related to some form of aerosol or marine haze. A correlation with major weather events, like the Monsoon season in the Indian ocean and possibly El Nino events is suspected, but has not been demonstrated. AIRS was launch into polar orbit on the EOS Aqua spacecraft on May 4, 2002.

Introduction

The primary objective of the Atmospheric Infrared Sounder (AIRS) (Aumann et al 2003) is the support of medium range weather forecasting with temperature and moisture vertical profiles and surface skin temperatures. The routine availability of global sea surface skin temperature with 0.1K absolute accuracy for the initialization of Global Circulation Models (GCM) is a long range goal of Numerical Weather Centers (NWC). Since 30 January 2001 the Real Time Global SST (RTG.SST) (Thiebaux et al. 2003) , developed by the National Centers for Environmental Prediction/Marine Modeling and Analysis Branch (NCEP/MMAB), is generated every 24 hours in support of mesoscale forecasting. The RTG.SST refers to the bulk temperature, i.e. the temperature at about one meter below the surface, roughly at the level of floating buoys. It is a blended product, consisting of the most recent surface reports and satellite data, interpolated with the GCM on a 0.5 degree global grid. Routine daily monitoring of the RTG.SST relative to the floating buoys indicates essentially zero global bias with standard deviation of 0.5K. Part of the on-orbit radiometric validation plan for AIRS included detailed comparisons with the RTG.SST. Extensive pre-launch testing of the AIRS radiometric calibration relative to a NIST certified blackbody showed (Pagano et. at. 2003) that the AIRS radiometric calibration for a uniformly illuminated scene between 220 K and 320 K is accurate to within 0.2K at all scan angles and all 2378 AIRS channels, with considerably better accuracy near the 308.3K temperature of the onboard precision radiometric reference source.

AIRS was launch into sun-synchronous polar orbit on the EOS Aqua spacecraft on May 4, 2002. The initial validation of the AIRS calibration within days after activation in orbit on 13 June 2002 was based on comparing the AIRS observed radiance with those calculated using the NCEP (National Center for Environmental Prediction) analysis under the relatively clear, but climatologically limited conditions of the summer Mediterranean ocean on 14 June 2002 (Aumann and Pagano 2002, Strow et al 2002). The results were very encouraging, but not reliable to better than 0.5K. The analysis of very large global data sets is required to make reliable statements approaching the 0.1K level. In the following we first describe the technique used by AIRS to make the sst measurements using the 2616cm-1 channel, sst2616. The advantage of the 2616cm-1 channels for precision surface measurements from space was first pointed out by Chahine (1978). We then discuss results pertaining to more than 250,000 sst2616 measurements during September 2002, the first month for which continuous observations from AIRS became available.

Approach

The retrieval of AIRS sea surface skin temperature requires two major steps:
1) The brightness temperatures measured at 2616 cm-1, bt2616, have to be corrected for atmospheric transmission and surface emissivity, resulting in sst2616.

2) A cloud-free data are required. This requires a cloud filtering algorithm or a cloud-clearing algorithm. Ultimately, the AIRS Unified Team Algorithm (Susskind et al. 2003) will generate cloud-cleared radiances. Until this algorithm becomes routinely available we use cloud filtering. This is acceptable for calibration evaluation and climate studies.

1. Correction for atmospheric transmission and surface emissivity

The atmospheric attenuation at 2616cm-1, almost entirely due to water vapor continuum, is very weak, but since accuracy at the 0.1K level is desired, atmospheric transmission has to be taken into account. Figure 1. shows the spectrum calculated for a US standard atmosphere (TSurf=299.7) between 2580 and 2680 cm-1 for a surface emissivity of 1.00 (upper curve with dots) and emissivity=0.98 (lower curve). Each dot represents one AIRS channels. The temperature measured at 2616cm-1, bt2616, is 299.4K , i.e. the atmospheric attenuation is only 0.3K. The nearby waterline at 2607 cm-1 measures a temperature of bt2607=295.4K, i.e. 4K colder than the measurement at 2616cm-1. The depth of the 2607cm-1 waterline relative to 2616cm-1, d2607, is a function of the amount of water vapor in the vertical column in the lower troposphere. This is the basis of the atmospheric transmission correction at 2616cm-1.

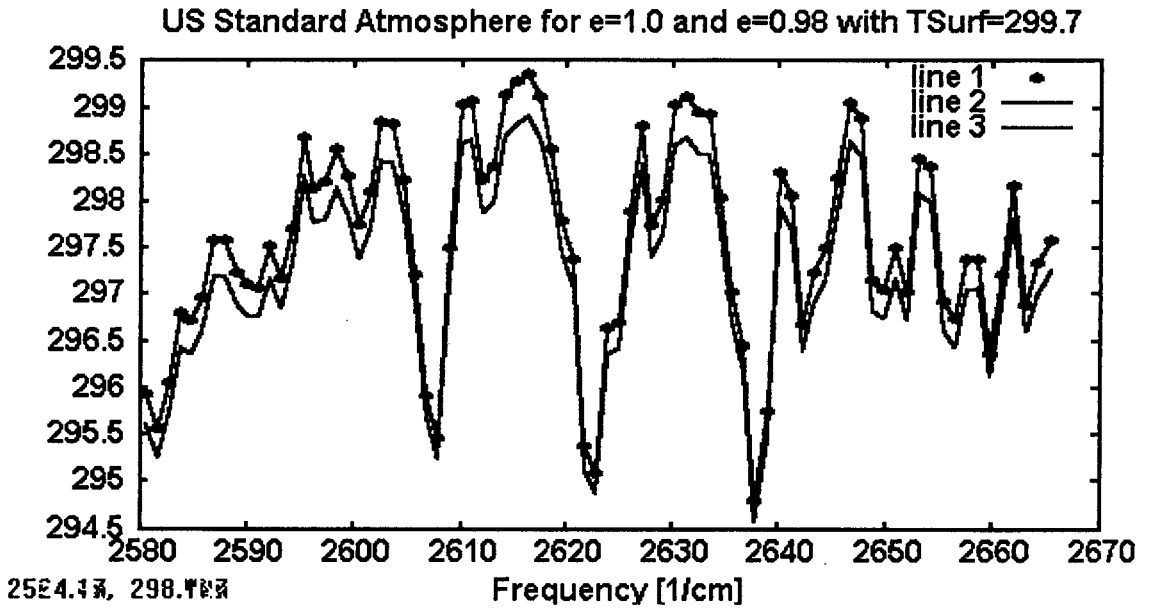

Figure 1. shows the 2580 to 2680 cm-1 region of the spectrum for a US standard atmosphere. Each point is the measurement of one of the 2378 AIRS spectral channels.

Figure 2 shows the atmospheric correction at emissivity 1.00 and 0.98 for twenty eight temperature profiles with TSurf>270K as function of d2607, calculated from the radiative transfer equations developed for AIRS (Strow et al. 2003). The correction at e=1.00 ranges from 0.1K for extremely dry conditions, 0.3K for the US standard atmosphere, to 0.8K under the extreme conditions of temperature and humidity encountered in the ITCZ. For these conditions d2607 increases from essentially zero to 8.6K. We now express

$$sst2616=bt2616+a0,i + a1,i*d2607+a2,i*d2607^2,\ i=1,2 \qquad \text{Eq.1}$$

where a0, a1 and a2 are deduced by fitting the radiative transfer calculations for the 28 climatological conditions for e=1.00 and e=0.98. The numerical fitting error is much less than 0.1K.

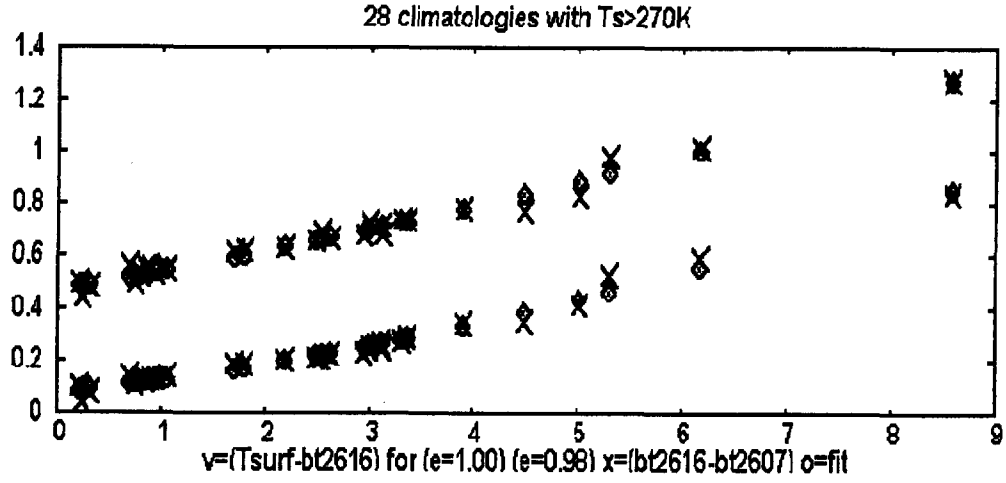

Figure 2. shows the atmospheric correction required as function of the predictor d2607. The circles are calculated based on a representative sample of 28 temperature and moisture profiles for a surface with unity emissivity (lower curve) and 0.98 emissivity (upper curve). The o-marks are a quadratic fit through the calculated points .

The emissivity of the sea surface is a function of satellite zenith angle (sza) and the wind speed. We use the emissivity data from Masuda et al. (1988), plotted in Figure 3 as function of sza and wind speed. We correct for the sza dependence, but assume a wind speed of 5 m/s. From Figure 2 we note the importance of an accurate emissivity correction: Each 1% drop in emissivity decreases the surface emission at 2616cm-1 by about 0.2K. If we want the correction to be more accurate than 0.1K , the emissivity has to be known to better than 0.5%. This point is reached at sza=45 degrees, assuming no uncertainty in the Masuda model. Since the number of cloud-free footprints decreases rapidly at |sza|>35 degree, the impact of the uncertainty on global statistics is not severe.

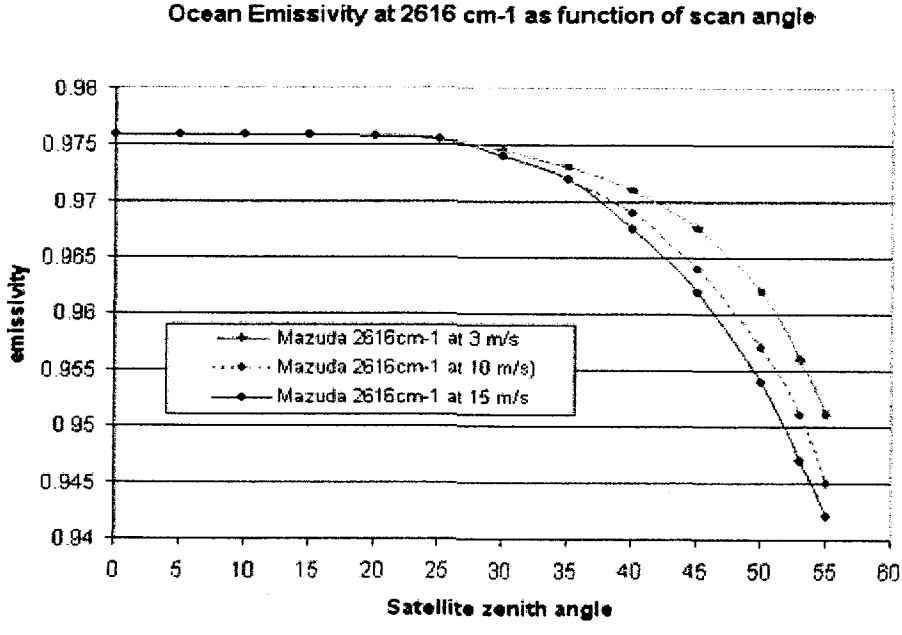

Figure 3. Emissivity of the sea surface at 2616 cm-1 as function of satellite zenith angle and wind speed.

The transmission correction for the appropriate value of the emissivity is calculated by interpolating the precalculated 0.98 and 1.0 emissivity cases. A Matlab code fragment in Figure 4. gives the numerical details.

```
disp('9 February 2003 emissivity correction');e2616=ones(size(bt2616));
v25=find(abs(sza_m)>25);
e2616(v25)=(cos((abs(sza_m(v25))-25).*0.6./57.3)).^0.4; % Mazuda v=5m/s
d2607=bt2616-bt2607;
a2616_1=0.052+0.05289.*d2607+0.002545.*(d2607.^2);
a2616_98=0.4075+0.10846.*d2607-0.000053.*(d2607.^2);
a2616e=a2616_1+(a2616_98-a2616_1).*(0.976.*e2616-1)./(0.98-1);
sst2616=bt2616+a2616e;
```

Figure 4. Numerical details of the emissivity and atmospheric transmission correction

Based on the coefficients of the fit one could deduce a nominal rms uncertainty of the sst2616 of 0.17K at |sza|<40 degrees. This ignores the effect of the error introduced by residual cloud contamination, which is discussed next.

2. Cloud Filtering.

If 1% of a 290K surface covered by the AIRS 13.5 km diameter footprint, was obscured by an optically thick cloud at 270K, the signal at the spacecraft would be reduced by 0.14K. A temperature of 270K is very typical for low stratus clouds. If a measurement accuracy of 0.1K is to be achieved, the elimination of any unrecognized cold bias due to cloud contamination at the 1% level is critical. An AIRS pixel is defined as cloud-free if the pixel passes a spatial coherence test and a low stratus cloud test.

a) Spatial Coherence test: Use of a spatial coherence test for the elimination of cloud contaminated fields of view was first discussed by Coakley and Bretherton (1982). This is an empirical approach, and the quality of the result depends on the the details of the implementation. The spatial coherence test uses a 3 x 3 pattern of AIRS footprints. This is illustrated in Figure 5. If bt2616(i), with i=1..9, is the brightness temperature measured at 2616cm-1 for the i-th pixels, then the center pixel passes the coherence test, if

(max(bt2616(i)-min(bt2616(i))< sc.

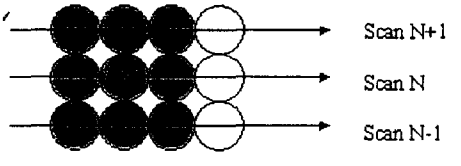

Figure 5. illustrates the spatial coherence test. If the differences between the nine pixels significantly exceed the value expected for a uniform scene measured with gaussian noise, then the center pixel is rejected as cloudy.

Theoretically, the lower the threshold, the less the cloud contamination is expected to be. The practically usable value of sc is a function of the NEDT of the channel. The NEDT at 2616 cm-1 for a 290K scene is 0.07K. Since the likely value of (max(bt2616(i)-min(bt2616(i)) in the presence of a totally homogeneous scene is approximately 3*NEDT=0.2K, sc=0.2K is the lowest usable threshold. For this study we use data with sc<0.5K. The value of sc is part of the record saved for each footprint. Figure 6. shows a histogram of the sc for data from the September 2002.

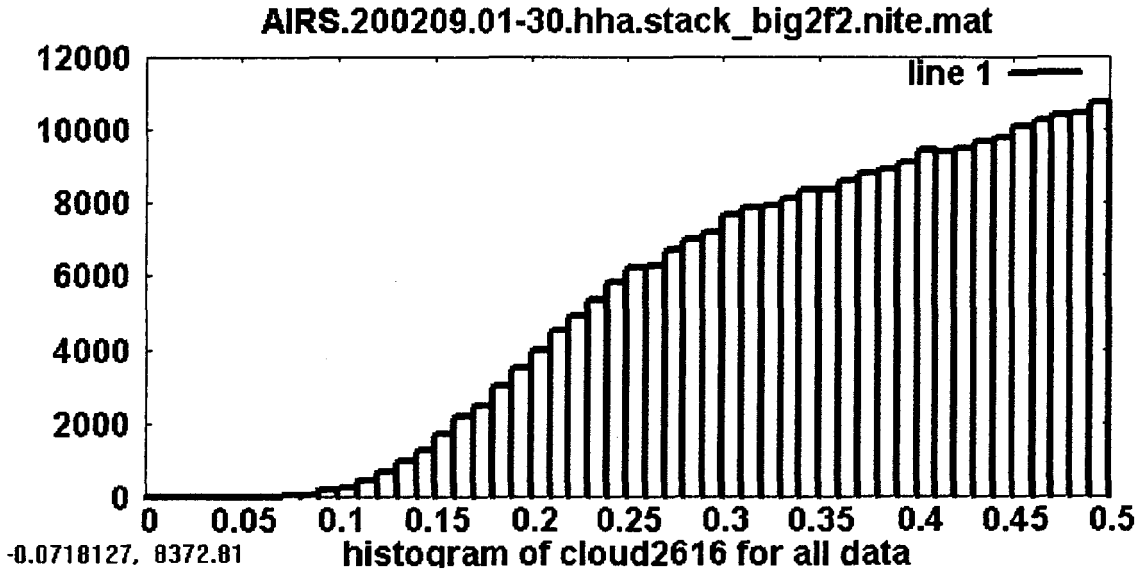

Figure 6. Histogram of the number footprints as function of sc. Footprints with sc<0.5Kare defines as "spatial coherence clear". The histogram goes to zero at 0.07K, the detector NEDT.

b) Low stratus test: A small fraction of the footprints passes the spatial coherence test, but is obviously cloud contaminated, because the observed brightness temperature is colder than the RTG.SST by typically 5 to 20 K. The weak water line at 2607cm-1 measures moisture in the lower part of the troposphere. It is normally in absorption above warm ocean. If part of the lower tropopause is cut off due to clouds, the line depth decreases and sometime goes into emission in the presence of a low stratus cloud cover. For the low stratus test we require that d2607>1K.

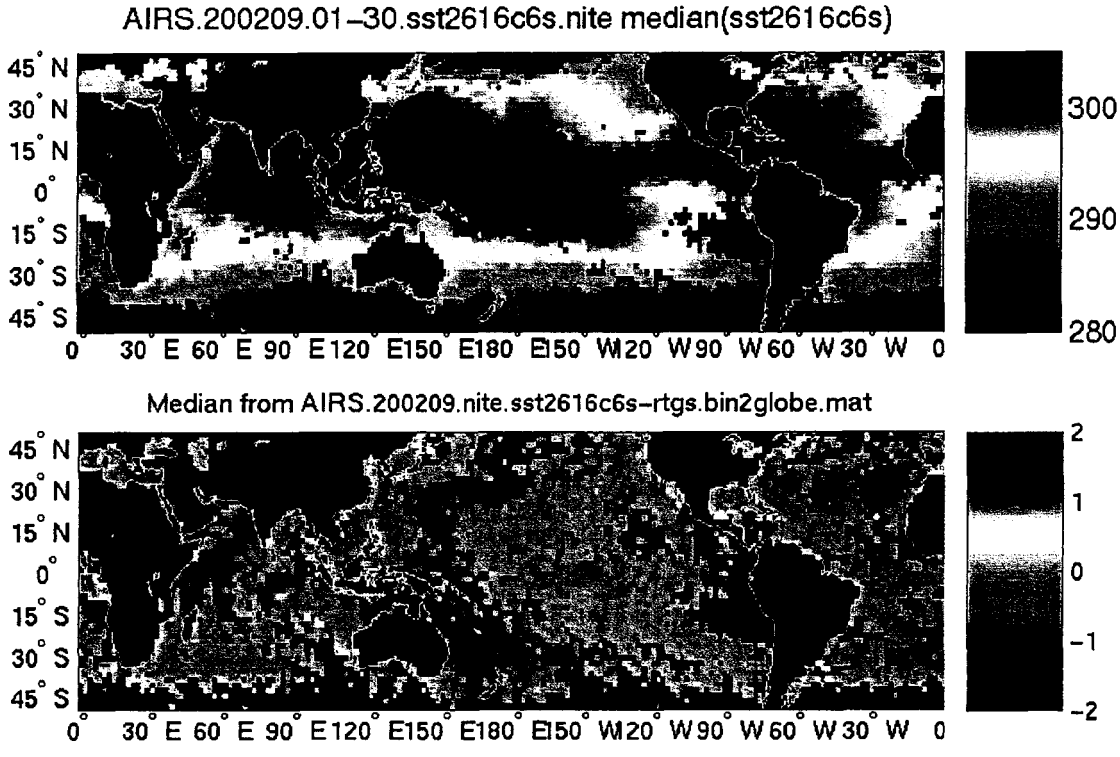

Figure 7. Top: False color image of sst2616 with 2 degree square bins between +/- 50 degree latitude using September 2002 data. Bottom: Image of sst2616-RTG.SST. Note the cold (dark) patterns.

Results

The AIRS data became available in the "operational mode" on 31 August 2002. Between September 1 and September 30, 2002 258,168 footprints passed the clear test over ocean. The top of Figure 7 shows a false color image of sst2616 created from these data with 2 degree latitude and longitude bins between +/- 50 degree latitude. Coastlines are outlined in white. The median value of the entries in each bin, typically 20 measurements per bin, is plotted, unless there are less than three entries, in which case no numerical entry is made. The dark spots in the ocean correspond to pixels which contain less than 3 measurements during the entire month of September 2002. The areas off the west coast of South America and South Africa are well known for their virtually permanent cloud cover.

In order to evaluate the sst2616 we compared each clear footprint with the nearest RTG.SST grid point for the appropriate day. The bottom Figure 7 shows the resulting image. The median (sst2616-rtg.sst)=-0.73K with standard deviation of 0.45K for the 258,158 matchups with the RTG.SST. 98% of the rtg.sst points agree with the AIRS sst2616 with -2.17K and +0.35K. In order to minimize the effect of potential outliers and population skew we use the width of the distribution which contains 68% of the population for the estimate of the standard deviation, but also quote the range which covers 98% of the data. Since 98% of a gaussian population would be contained within +/- 2.35 sigma, the 98% population standard deviation of sst2616-rtg.sst = 0.54K. This is 0.09K larger than the 68% population sigma, but still indicates a fairly clean distribution.

The statistical analysis of all "clear" data relative to the RTG.SST is statistically somewhat skewed for two reasons:
1. In some clear areas the 55 km spacing of the RTG.SST grid may cause several AIRS 15 km footprints to be matched up with the same RTG.SST point.
2. The clear pixels are not at all uniformly distributed on the globe, but are concentrated in a narrow region along the equator, which is extremely warm and humid.
These effect can be reduced by analyzing the statistical distribution of the binned difference between sst2616 and the RTG.SST. The 2 degree bin map contains 9000 bins, 5608 of these are ocean bins, and 5035 have a sst2616 measurement. For these 5035 bins the sst2616 is 0.68K colder then the RTG.SST, with a standard deviation of 0.31 K, with 98% of the population in the -1.7K to +0.2K range.

Discussion

Several point can be made by inspection of the (sst2616-RTG.SST) image:
1. The scale from -2 to +2K contains more than 99% of the points. The fact that the AIRS sst2616, which is based entirely on first principles, agrees with the RTG.SST to within a fraction of a degree between +/-50 degree latitude is a very impressive tribute to the quality of the RTG.SST product and the absolute accuracy of the AIRS measurements.
2. Most areas in the image show a small cold bias between sst2616 and RTG.SST. There are two effects which make the sst2616 colder than RTG.SST: The fact that the RTG.SST reports the bulk temperature, while sst2616 measures the skin, produces a statistical cold bias of about 0.18K (Donlon et al. 2002) . In addition, since the RTG.SST is a day/night averaged product, while the AIRS sst2616 measurements are from night time observations only, a cold bias of between 0.15K and 0.2K is expected (P. Minnett, 2003). The expect sst2616-rtg.sst bias thus ranges from 0.33K to 0.38K, compared to the observed bias of 0.68K. Between 0.3K to 0.35K of the cold bias is unexpected.
3. There are large spatially correlated areas off the east coast of Africa, in the Arabian Sea, in the Coral Sea off the East coast of Australia and others, where the sst2616 is significantly colder than the RTGSST. Of the 5035 pixels with sst2616, 908 (18%) are more than 1K colder than the RTG.SST.

Analysis of sst2616-RTG.SST as function of scan angle shows that the observed cold bias has the characteristics of an absorbing atmospheric layer. This is shown in Figure 8. The diamonds represent the medians of the observed values in four degree sza bins, the crosses are a plot of bias=-0.30-0.37/cos(sza). The scan angle independent component of -0.3K is within the range of the expected sst2616-RTG.SST difference, while the -0.37K component is due to absorption by a some atmospheric layer.

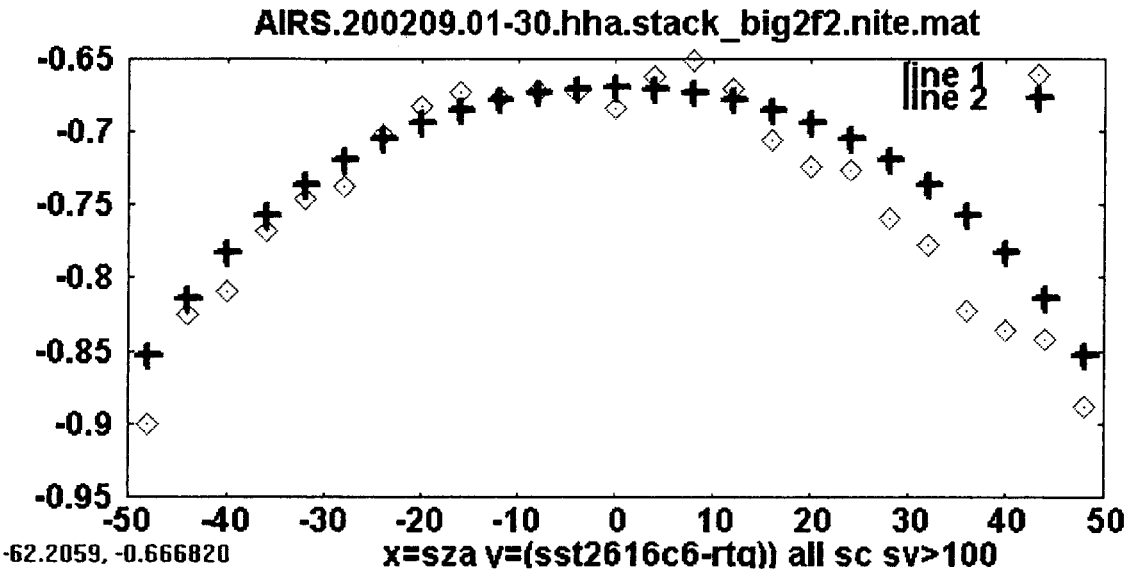

Figure 8. sst2616-RTG.SST as function of scan angle shows the characteristic 1/cos(sza) dependence of an absorbing atmospheric layer.

This interpretation holds for the global average as well as the regions which show significantly more absorption, such as the area of the Coral Sea, bounded approximately by -40 degree< latitude < -10 degree, 150E< longitude< 180E. For the Coral Sea area we find sst2616-rtg.sst = -1.25K with standard deviation of 0.53K for 13334 points. Figure 9. shows a plot of these points as function of sza. The circles represent the measurements in 4 degree bins, the crosses are a plot of bias=-0.4-0.7K/cos(sza). Although the sparseness of the data makes this fit not as crisp as the fit of the global data, the absorbing layer in the Coral Sea appears to be roughly twice as strong as the global average.

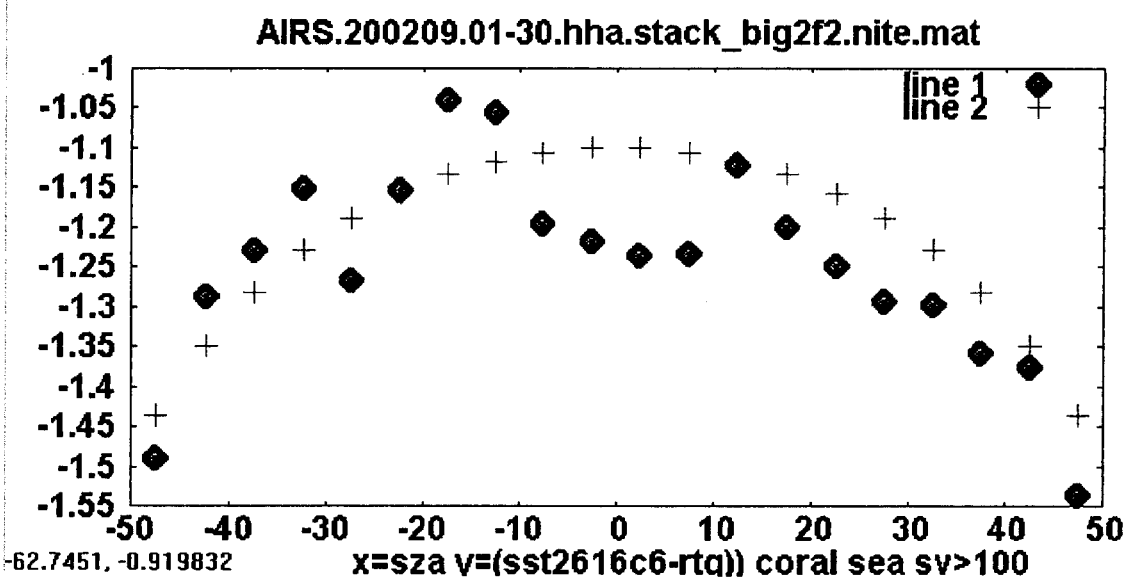

Figure 9. sst2616-RTG.SST for the Coral Sea area, bounded by -40 degree< latitude < -10 degree, 150E< longitude< 180E, shows a 1/cos(sza) dependence.

A component of the cold bias is sensed by the spatial coherence test. This is shown in Figure 10. As the spatial coherence parameter increases from 0 to 0.5K (sst2616-rtg.sst) changes from -0.62K to -0.81K. At least from a statistical viewpoint, data which pass the spatial coherence test with sc=0.5K are 0.2K too cold due to cloud contamination. Since the average sc of the all September 2002 data is 0.35K, 0.12K of the observed 0.37K cold bias may simply be cloud filter related.

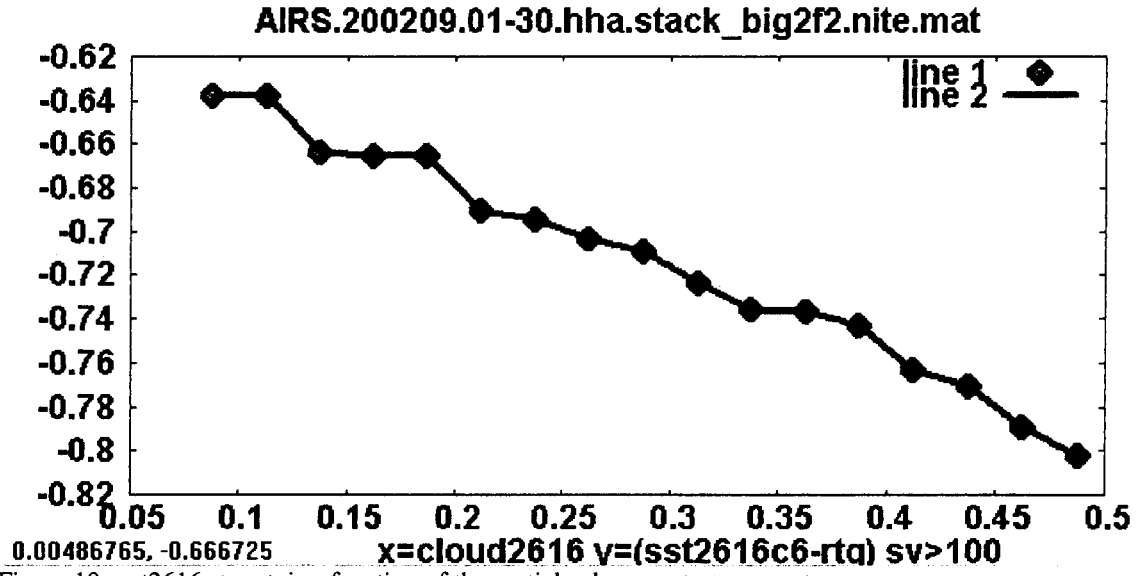

Figure 10. sst2616-rtg.sst is a function of the spatial coherence test parameter.

If simple cloud contamination was the correct interpretation of the entire unexpected cold bias, we would expect a strong correlation where there is a larger bias. Figure 11 shows (sst2616-rtg.sst) as function of sc for the Coral Sea region. There are 13334 "clear" points in the Coral Sea. Unlike the unambiguous correlation between sc and (sst2616-rtg.sst) in the global case, there is no significant correlation for the comparison limited to the Coral Sea area. Only results from sc bins with more than 50 entries are shown.

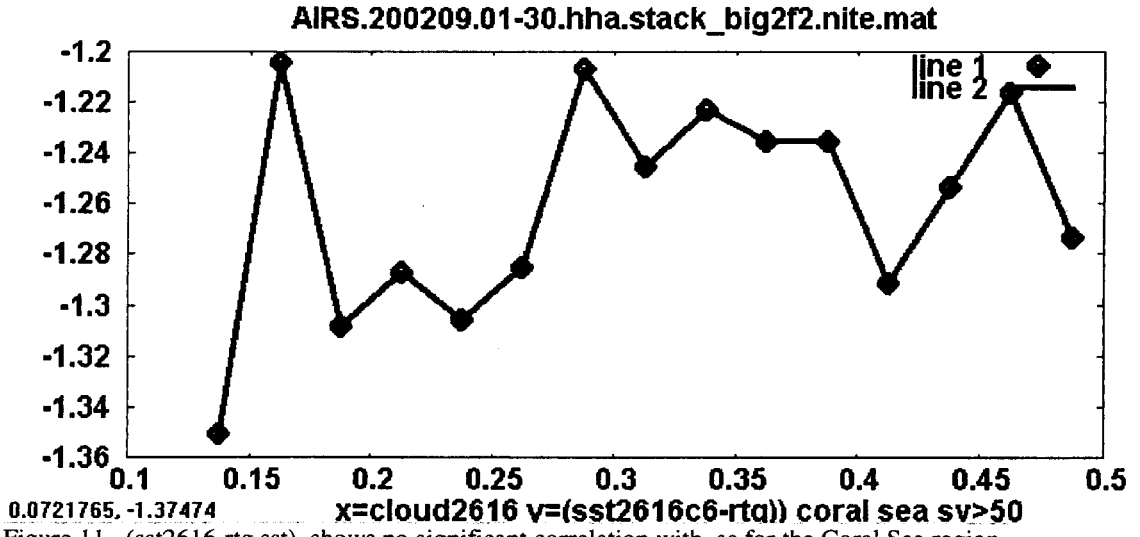

Figure 11. (sst2616-rtg.sst) shows no significant correlation with sc for the Coral Sea region.

This suggests that we are dealing with two different effects: Contamination by "conventional clouds" , perhaps trade cumulus, which follows the expected sc dependence, and absorption by an atmospheric layer which is horizontally homogeneous on a much larger scale than 50 km, which may be some form of haze or perhaps marine aerosol. The

undetected effect of both on the retrieved sst would explains the unexpected difficulties encountered by previous investigators, such as ATSR (Jones et al. 1996), attempting physical retrievals of the sst.

The search for clues as to the nature of this absorbing layer is ongoing. AIRS sst measurements since September 2002 show changes in the patterns of the enhanced absorbing regions in the Indian ocean on a months time scale, suggesting a correlation with the Monsoon season. Issues still to be explored are potential cirrus and silicate dust in the AIRS "clear" footprints, surface temperature, (sst2616-rtg.sst) and wind speed correlations, and evaluation of sst measurements using AIRS window channels at 1231cm-1 and 900cm-1 to evaluate particle size effects.

The presence of an absorbing layer which varies globally from zero to 0.7K and more, with a global average of 0.37K presents an major challenge to measurements of the sea surface skin temperature from space. If the effect of cloud contamination on sst2616 were to be corrected with an empirical constant offset or a sc dependent offset, the bias of sst2616 relative to the RTG.SST would be reduced, but the rms accuracy of sst2616 would still be limited to the rms value of the regional and possibly seasonal variability of the effect, which is about 0.3K. If the unaccounted for cloud contamination is related to major weather effects, like the Indian Monsoon, or El Nino type effects, the constant will require empirical seasonal updates.

AIRS was designed for an on-orbit lifetime of seven years. This is a large enough time span for time lagged correlations of this effect between geographical areas, like El Nino events. The identification of such a correlation would present an opportunity for long range weather forecasting.

Conclusions.

AIRS measurements of the ocean skin surface temperature from first principles for the month of September 2002 agree surprisingly well with the RTG.SST. The standard deviation is only 0.44K, but, after accounting for an expected diurnal and skin-bulk effect, there is an unexplained global bias of about 0.37/cos(sza) suggestive of absorption by an atmospheric layer, possibly dust, aerosol or marine haze. The presence of this absorber in large scale features, such as in the Coral Sea, with persistence on a months timescale, may be spatially time lag correlated between geographical areas to major effect, like El Nino events. This present an opportunity for long range weather forecasting. It also presents a significant hurdle to measurements of the sea surface skin temperature at the 0.1K level.

Acknowledgements

Peter Minnett (U. Miami) from the MODIS SST team provided helpful discussion on the skin-bulk gradient, diurnal effects and the potential effects of rain on sst skin measurements. Tom Pagano and the calibration team, including Ken Overoye from BAE Systems get credits for a first class pre-launch calibration and Level 1b software for AIRS. This work was carried out at the Jet Propulsion Laboratory, California Institute of Technology, under NASA contract.

References

Aumann, H.H. , M.T. Chahine, C. Gautier, M. Goldberg, E. Kalnay, L. McMillin, H. Revercomb , P.W. Rosenkranz , W. L. Smith , D. H. Staelin, L. Strow and J. Susskind, "AIRS/AMSU/HSB on the Aqua Mission: Design, Science Objectives, Data Products and Processing Systems", IEEE Transactions on Geoscience and Remote Sensing, Feb 2003, V.41,#2, 253-264.

Thiebaux, Jean, Eric Rogers, Wanqiu Wang, and B. Katz, "A New High-Resolution Blended Real-Time Global Sea Surface Temperature Analysis", BAMS 2003, V.84, #5, 645-656.

Pagano, T.S., H. H. Aumann, D. Hagan and K. Overoye, "Prelaunch and In-Flight Radiometric Calibration of the Atmospheric Infrared Sounder (AIRS), IEEE Transactions on Geoscience and Remote Sensing, Feb 2003, V.41,#2, 265-273.

Aumann, H. H. and T. S. Pagano, "Early results from AIRS on EOS", Proc. SPIE Intern. Symp. on Remote Sensing, Crete, Greece 23 September 2002.

Strow, L. L., S. E. Hannon, S.DeSouza-Machado, and H. Motteler, "Validation of the AIRS radiative transfer algorithm using ECMWF data fields", Proc. SPIE Intern. Symp. on Remote Sensing, Crete, Greece 23 September 2002.

Chahine (1978?) Discussion of using 2616cm-1 for sst measurements.

Susskind, J., C. D. Barnet, and J. M. Blaisdell, "Retrieval of Atmospheric and Surface Parameters from AIRS/AMSU/HSB Data in the Presence of Clouds", IEEE Transactions on Geoscience and Remote Sensing, Feb 2003, V.41,#2, 390-409.

Strow, L.L., S. Hannon, S. DeSouza-Machado, H.E. Motteler and D. Tobin, "An Overview of the AIRS Radiative Transfer Model", IEEE Transactions on Geoscience and Remote Sensing, Feb 2003, V.41,#2, 303-313.

Masuda, K., T. Takahima, and Y. Takayama, (1988) "Emissivity of pure and sea water from the model sea surface in the infrared window regions". Remote Sensing of the Environment, 24, pp313-329.

Coakley, J.A., and F.P. Bretherton (1982) "Cloud cover from high resolution scanner data: Detecting and allowing for partially filled fields of view", J. Geophys. Res. 87, 4917-4932

Donlon, C.J., P.J. Minnett, C. Gentemann, T.J. Nightingale, I.J. Barton, B. Ward and M.J. Murray ,"Toward Improved Validation of Satellite Sea Surface Skin Temperature Measurements for Climate Research', J.of Climate, 15, pp.353-369 (2002)

Minnett, R. 2003 pers. communication

Jones, M. S, M. A. Saunders and T. H. Guymer, "Global remnant cloud contamination in the along-track scanning radiometer data: Source and removal" J.G.R.101, pp.12,141-12,147 (1996).